

This is the authors' version (pre peer-review) of the manuscript: C. L. Pereira et al 2D Materials
<https://doi.org/10.1088/2053-1583/ab0b23>

That has been published in its final form: <https://iopscience.iop.org/article/10.1088/2053-1583/ab0b23/meta>

Reversible doping of graphene field effect transistors by molecular hydrogen: the role of the metal/graphene interface

C. L. Pereira^{1,2,*}, A. R. Cadore^{1,2,*}, N. P. Rezende¹, A. Gadelha¹, E. A. Soares¹, H. Chacham¹, L. C. Campos¹, R. G. Lacerda^{1,*}

¹*Departamento de Física, Universidade Federal de Minas Gerais, Belo Horizonte, 30123-970, Brasil*

²*These authors contributed equally to this work.*

^{*}*Electronic mail: cintialpfisica@gmail.com; alissoncadore@gmail.com, rlacerda@fisica.ufmg.br*

In this work, we present an investigation regarding how and why molecular hydrogen changes the electronic properties of graphene field effect transistors. We demonstrate that interaction with H₂ leads to local doping of graphene near of the graphene-contact heterojunction. We also show that such interaction is strongly dependent on the characteristics of the metal-graphene interface. By changing the type metal in the contact, we observe that Ohmic contacts can be strongly or weakly electrostatically coupled with graphene. For strongly coupled contacts, the signature of the charge transfer effect promoted by the contacts results on an asymmetric ambipolar conduction, and such asymmetry can be tunable under interaction with H₂. On the other hand, for contacts weakly coupled with graphene, the hydrogen interaction has a more profound effect. In such situation, the devices show a second charge neutrality point in graphene transistor transfer curves (a double-peak response) upon H₂ exposure. We propose that this double-peak phenomenon arises from the decoupling of the work function of graphene and that of the metallic electrodes induced by the H₂ molecules. We also show that the gas-induced modifications at the metal-graphene interface can be exploited to create a controlled graphene p-n junction, with considerable electron transfer to graphene layer and significant variation in the graphene resistance. These effects can pave the way for a suitable metallic contact engineering providing great potential for the application of such devices as gas sensors.

1 – INTRODUCTION

Graphene is a two-dimensional (2D) material that is well known by its remarkable thermomechanical and electronic properties. The ability to modulate and control graphene electronic properties in different and efficient ways are of paramount importance for the commercial realization of graphene applications [1–4]. For instance, graphene field effect transistors (GFETs) have demonstrated great potential for applications in several areas such as high-frequency transistors [2,5], biological and chemical sensors [6,7], and in a variety of optoelectronic devices [8–11]. In the GFET configuration, an electric current between the source and drain terminals is modulated by the application of a gate potential [1,5,12,13]. In this context, it is well known in the microelectronics industry that electric transport between the conducting channel and metallic electrodes plays an important role in the device characteristics and performance [14,15]. Thus, an intensive effort has been devoted to understand and improve the electrical junction between the metallic electrodes and graphene [16–22]. Typically, in a metal-semiconductor junction, there is a Schottky-barrier that actively affects the electronic device properties [3,5]. However, in a metal-graphene junction, even an Ohmic contact can passively play a role in device conduction due to unusual effects originated from the quantum electronic properties of graphene [23]. Moreover, graphene depicts a zero-gap and approximately linear energy dispersion near the vicinity of the Fermi level [4,24]. These features provide an ambipolar electronic conduction, and GFET transfer characteristics (conductance versus gate voltage curves) typically displaying a “V-shaped” form [1]. Thus, the minimum of conductivity (or maximum of resistivity) of the transfer curve corresponds to the crossing of the Fermi level at the Dirac point in the graphene electronic band structure [4]. Around this point, where the graphene density of states vanishes, the concentration of thermoactivated electrons is equal to that of holes being labeled as the charge neutrality point (CNP) [1,4]. In general, there is only one CNP in the transfer characteristics of GFETs [1,2]. Nevertheless, several experimental works have demonstrated that graphene devices can exhibit multiple maxima of resistance depending on

This is the authors' version (pre peer-review) of the manuscript: C. L. Pereira et al 2D Materials
<https://doi.org/10.1088/2053-1583/ab0b23>

That has been published in its final form: <https://iopscience.iop.org/article/10.1088/2053-1583/ab0b23/meta>

external environmental conditions, contaminations, and device structuring [25-31]. This means that, in such systems, there are adjacent regions of graphene with different local density of charges, or even the existence of heterojunctions (regions p-type doped nearby regions n-type doped) as it is theoretically predicted [15]. A double-CNP in the transfer curve of a GFET can also be intentionally created using a double-gate structure that enables setting the density of charges at different regions of the graphene channel independently [34,35]. Apart from this case, all the other processes that create the double-CNP are irreversible, which limits the device electrical performance and applicability. Therefore a further understanding of these phenomena, as well as the use of it in a controllable and tunable way is still lacking.

In this work, we systematically investigate how and why molecular hydrogen tunes the electrical properties of graphene devices. We show that the interaction with H₂ promotes a local doping of graphene at the metal-graphene interface, which is strongly dependent on the characteristics of the device. For instance, by changing the type of metal-graphene heterojunction, we observe that Ohmic contacts can be strongly or weakly coupled electrostatically with graphene. In a strongly coupled heterojunction, there is a Fermi level pinning effect at the metallic leads fixing the charge density nearby. Consequently, graphene field effect transistors show an asymmetric ambipolar conduction, and such asymmetry can be tunable under interaction with H₂ [23]. On the other hand, in devices with metallic leads weakly coupled with graphene (such as Au/Cr₂O₃ electrodes), hydrogen interaction at the metal/graphene interface generates a second charge neutrality point in graphene transfer curves (a double-CNP feature). We propose that this double-peak phenomenon arises from the decoupling of the work function of graphene and that of the metallic electrodes under interaction with H₂. The induced double-CNP or “M-shaped” form observed is completely controllable and reversible via molecular hydrogen (H₂) exposure. Those effects provide considerable electron transfer to graphene layer and large variation in the graphene resistance providing an alternative approach for suitable engineering at graphene/contact interfaces with great potential for application of gas sensors.

2 - EXPERIMENTAL METHODS

For a better understanding of the role of hydrogen on the electronic properties of GFET, we built several devices with different parameters: device geometry, channel lengths, and types of metallic electrodes. Graphene devices were prepared using monolayer graphene produced via mechanical exfoliation on SiO₂(300nm)/Si substrate, where heavily doped silicon issued as the back-gate electrode [1]. Electron beam lithography and oxygen plasma etching were used to define the graphene shape. The metallic electrodes of all devices were designed by electron beam lithography, followed by thermal metal deposition and lift-off. Here, we fabricated GFETs with pure Au (30nm), Au/Cr (30nm/1nm) and Au/Cr₂O₃ (30nm/~1nm) as metal-type electrodes, forming the metal-type/graphene/SiO₂/Si structures. GFETs were also fabricated with 5nm and 10nm Cr₂O₃ thick for the Au/Cr₂O₃ transistors. In all these devices, the metallic electrodes were defined and deposited on top of the graphene channel, as illustrated in the top panels of Figures 1(a) and 1(c)-1(f). However, GFETs were also fabricated by transferring graphene on top of pre-prepared Au/Cr (30nm/1nm) electrodes, as illustrated in the top panel of figure 1(b), forming the graphene/Au/Cr/SiO₂/Si structures.

Our standard GFETs devices were prepared with several materials as contacts, and keeping the same graphene channel length ($L = 1\mu\text{m}$), channel width ($W = 3\mu\text{m}$), and electrodes length ($d = 1\mu\text{m}$). In the inset of figure 2(b) we illustrate the definition of electrode length, d . Additional devices were prepared to investigate the effects of the contact length, graphene channel length, and contact resistance on the formation of secondary CNPs. Accordingly, GFETs with Au/Cr₂O₃ electrodes, which show tunable secondary CNPs, were prepared at several other configurations: (i) GFETs with several electrodes lengths (from $d = 0.25\mu\text{m}$ up to $d = 2\mu\text{m}$, fixing $L = 1\mu\text{m}$ and $W = 3\mu\text{m}$ – see inset in figure 2(b)); (ii) GFETs with several graphene channel lengths (from $L = 1\mu\text{m}$ up to $L = 10\mu\text{m}$, keeping $d = 1\mu\text{m}$ and $W = 3\mu\text{m}$ – see inset in figure 2(c));

(iii) GFETs in Hall bar geometry, where we can ignore the influence of contact resistance[20,23]. In this geometry, we also measure the electronic properties of the device in a non-invasive (figure 1(e)) and invasive (figure 1(f)) configuration [20,23]. Finally, the formation of the Cr_2O_3 instead of Cr as a sticking layer underneath the gold contacts was produced by intentional oxidation of the chromium after deposition by thermal evaporation. For this process, immediately after the chromium deposition (~ 1 nm), usually performed at pressures around 2×10^{-6} Torr, the thermal evaporation chamber was opened to the environment for 30min and then pumped down back to 2×10^{-6} Torr before the gold deposition. Such an oxidation process of Cr was tested and characterized before we implemented it as our device preparation recipe. The oxidized materials (~ 1 nm of Cr_2O_3) were verified by atomic force microscopy (AFM) and X-ray photoelectron spectroscopy (XPS) (see Supporting Information).

After fabrication, each device was inserted into a homemade gas system tube equipped with heater and mass flow controllers, which enables the control of the temperature, from $T = 25^\circ\text{C}$ up to $T = 200^\circ\text{C}$, gases flow (Argon (Ar) and H_2) with hydrogen concentrations ($[H_2]$), from $[H_2] = 0.5\%$ up to $[H_2] = 50\%$ inside the chamber at atmospheric pressure. Before carrying out the electrical measurements, each device undergoes to a thermal conditioning process that consists on keep the devices at a temperature of $T = 200^\circ\text{C}$ under a flow of 300sccm of ultrapure Ar for 8h. This process is known to remove absorbed water molecules, impurities and contaminating gases from the graphene surface [36–38]. For the electrical characterization, we performed mainly two-probe measurements using the standard lock-in techniques, keeping fixed the frequency at 17Hz and current bias (I_{SD}) between the source (S) and drain (D) terminals of $I_{SD} = 1\mu\text{A}$, while we measured the voltage drop (V) in between both electrodes as illustrated in the top panel of figure 1(a). However, for the Hall bar geometry, the same parameters were used in between source and drain, while the voltage was measured in the inner electrodes as illustrated in the top panel of figure 1(e). Finally, for all devices, the total device resistance (R) was obtained by applying Ohm's law.

3 - RESULTS AND DISCUSSION

We start by showing typical transfer curves of a GFET and how H₂ modifies graphene electrical properties. In figures 1(a)-(d), we present data of two-probe measurements of transfer curves ($R \times V_G$) at $T=200^\circ\text{C}$ of graphene devices with contacts made of Au, Au/Cr and Au/Cr₂O₃. Note that graphene is contacted with Au electrodes in different ways. In figure 1(a), Au contacts are at the top of graphene, while in figure 1(b), graphene is at the bottom of the Au electrodes. Firstly, we would like to stress that in all devices characterized graphene main channel are n-type doped. This can be seen by the fact that the CNP locates at negative gate potentials. Such charge transfer effect depends mainly on the activation of surface dangling bonds in the SiO₂ by thermal conditioning, which is not controllable, explaining why the CNPs for different devices are not at the same gate voltage [36,39]. Secondly, the graphene conductance is ambipolar around the charge neutrality point, meaning that at the left side of the CNP, the electrical conduction is carried out by positive charge carriers (holes) whereas at the right side of the CNP the conduction is executed by negative charge carriers (electrons). Moreover, other information can be extracted by asymmetric transfer curves. If the transfer curve shows a larger resistance at the right side of the CNP, graphene at the contact interface is p-type doped promoting a preferential scattering of electrons [17,20,23]. Similarly, if the transfer curve shows a larger resistance at the left side of the CNP, the opposite applies, and we can infer that graphene at the contact interface is n-type doped scattering holes more efficiently than electrons. By carefully analyzing figures 1(a)-(d), one can see that there is a preferential scattering of electrons in absence of H₂ (all metallic contacts naturally promote a p-type doping of graphene near the leads). This statement is more evident in graphene/Cr/Au devices as shown in the black curve of figure 1(c) [17,20,23]. However, under exposure to H₂ (red curves in figures 1(a)-1(c)), there is an inversion of the asymmetry of the transfer curves [23]. In these circumstances, the metallic contacts promote a n-type doping of graphene in the region near the contacts and resistance at the left side of the CNP is larger than at

the right, of one compares the same density of charge. Additionally, under interaction with H₂, in all devices the CNP shifts towards more negative values of the gate potential, indicating a global electron transfer to the graphene. Previous works have justified similar charge transfer processes via H₂ dissociation and subsequent interaction of the atomic hydrogen with the graphene channel, causing the negative charge transfer and leading to chemical and permanent changes on the GFETs [25,40,41]. However, as we will discuss next, we do not observe permanent changes on the graphene electrical properties induced by H₂, and the idea of a hydrogenation process can be disregarded.

Now, by comparing the results presented in figures 1(a)-1(d) it is clear that the CNP shifts (ΔV_G) are not the same for all devices. These data indicate that the charge density transferred via interaction with H₂ depends on both the metal-type used and on the electrode position on the graphene channel (top or bottom). In this context, some features can be highlighted. Firstly, the largest charge transfer occurs in graphene devices contacted with pure Au (as we will discuss later, the charge transfer is proportional ΔV_G). Secondly, in GFETs with Au/Cr₂O₃ electrodes, as shown in Figure 1(d), in addition to the CNP shift, there is a formation of a second “peak” in the $R_{xx}V_G$ curves when the device is exposed to H₂ (red curve in figure 1(d)), resulting in a “M-shaped” curve. Here, it is important to mention that all data depicted in figures 1(a)-1(d) are taken from graphene devices with the same geometry (graphene channel length, width and electrodes length).

Now, we state that all effects discussed above can be addressed to charging effects at the graphene/metallic contact region. A demonstration that the graphene main channel is not becoming charged directly due to a interaction with H₂ is understood in measurements of devices prepared in a Hall bar geometry, as shown in figure 1(e). In such geometry, it is well-known that the contribution from the contact resistances can be disregarded [20,23]. Indeed, we do not observe any significant charging effect under H₂ exposure, even using Au/Cr₂O₃ electrodes. A similar result is described in a previous work using Au/Cr electrodes [23]. Nevertheless, when the

same device is measured in a two-probe configuration, the second CNP appears as well as the electron charge transfer, as it is shown in figure 1(f). We emphasize that the double-CNP occurs in all devices while keeping the current bias very low ($I_{SD} = 1\mu\text{A}$), suggesting that a second CNP does not appear as a result of charge trapped in the vicinity of the drain at the graphene/SiO₂ interface during a current bias stress [42]. Moreover, we also show in the Supporting Information an investigation of the double-CNP by measuring the hysteresis on the GFETs. Such experiments strongly indicate that contributions from trapped charges at the substrate [12,42,43] on the formation of the second CNP and charge transfer can be neglected. In summary, our experiment suggests a strong correlation between the generation of the secondary CNP via charging effects at the metal-graphene interfaces, which also may affect graphene contact resistance.

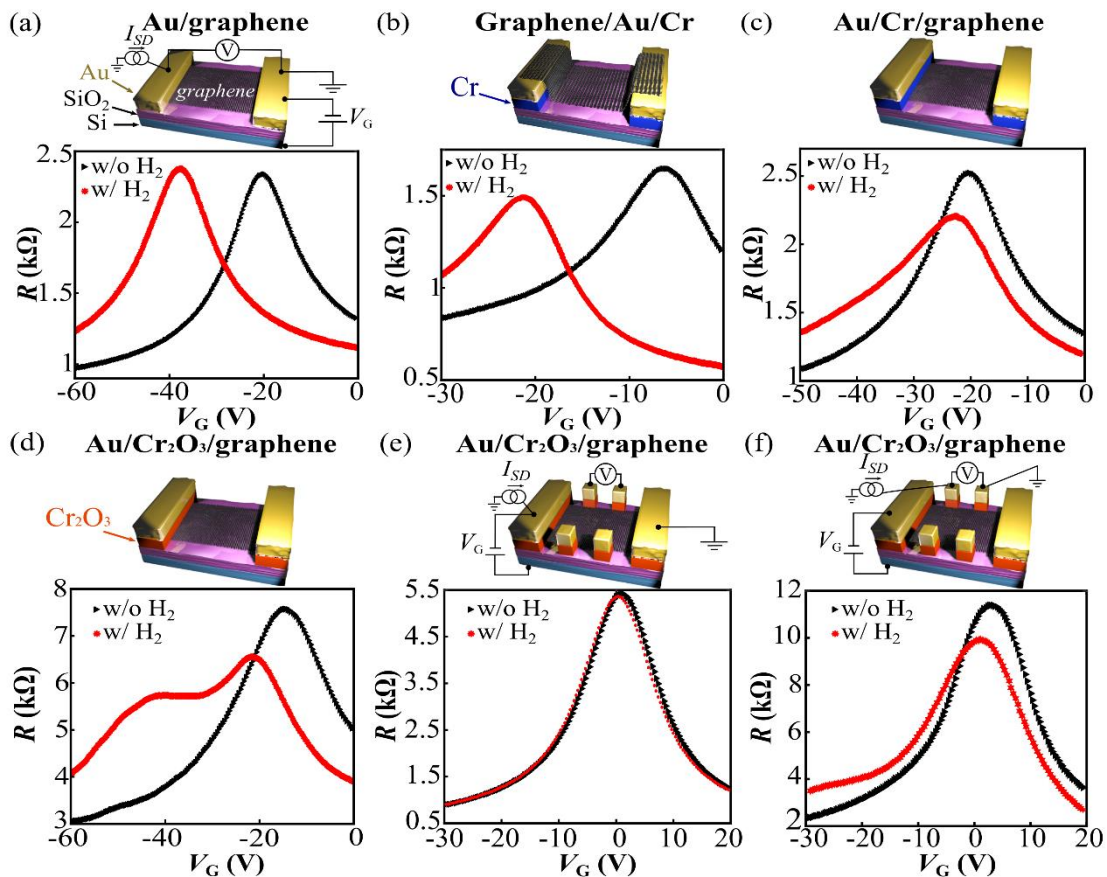


Figure 1. Measurements of two-probe resistance (R) as a function of back-gate voltage (V_G) under H₂ exposure for GFETs with different metal-type electrodes: pure Au/graphene (a), graphene/Au/Cr (b), Au/Cr/graphene (c), and Au/Cr₂O₃/graphene (d) on top of SiO₂/Si substrates. All devices are designed with the same graphene geometry ($L = 1\mu\text{m}$ and $W = 3\mu\text{m}$) and electrodes length ($d = 1\mu\text{m}$). (e) Four-probe and

(f) two-probe $R \times V_G$ curves for a GFET fabricated in Hall bar geometry with Au/Cr₂O₃ electrodes. All measurements presented in this figure are performed at $T = 200^\circ\text{C}$ and the data under $[H_2]=20\%$ exposure (red curves) are performed after 1h of gas exposure, while the black curves are measurements in pure argon, before turning on the molecular hydrogen. The insets in the figures illustrate the metal-type used in the fabrication process, the position of the graphene layer in the GFETs, the device geometry and the configuration for the electrical characterization.

It is important to address possible changes on the contact resistance when the device is exposed to H₂. Several works [14,44–46] propose that tunneling across the metal-graphene interface should dominate the charge injection from the metal into the underlying graphene in devices with Ohmic contacts. Besides that, changes on the transmission probability could change the contact behavior from Ohmic to non-Ohmic, also resulting in the observation of multiple CNPs [44–46]. Therefore, we show in figure 2(a) measurements of $I_{SD} \times V_{SD}$ for a device with Au/Cr₂O₃ electrodes before (blue curve) and after (red curve) gas exposure at $T = 25^\circ\text{C}$ and $[H_2] = 20\%$. One can note that the Ohmic behavior (linear relation between $I_{SD} \times V_{SD}$) of the device is not affected by the molecules. We only note a change on the slope of the curve shown in figure 2(a), which can be associated with the charge transfer to graphene channel, as demonstrated and discussed in figure 1(d). Such linearity implies that the oxide layer deposited does not form any detectable Schottky barrier in our devices. In addition, under interaction with H₂ there is a significant charging effect but the contact region between graphene and Au/Cr₂O₃ is still Ohmic for any value of gate bias applied (see Supporting Information). Also, in the Supporting Information, we present the $I_{SD} \times V_{SD}$ curves for all other devices with different metallic electrodes where a linear response is obtained in all of them (with or without H₂ interaction).

Now we investigate how the formation of multiple CNPs under interaction with H₂ depends on the device geometry. It has been reported that the two peaks in the $R \times V_G$ curves can be associated with the contact area and the length of the graphene channel [47,48]. In such experiments, the nature of contacts, without the presence of any type of gas, might be causing a local charging effect on the graphene underneath the electrodes. So, in figures 2(b) and 2(c) we

present curves of the resistivity ρ as a function of the carrier density n , for devices with several Au/Cr₂O₃ electrode lengths (figure 2(b)) and graphene channel lengths (figure 2(c)) after H₂ exposure. Here, the resistivity is calculated as $\rho = RW/L$, while the carrier density is obtained by $n = C(V_G - V^{\text{CNP}})/e$, where C is the graphene device capacitance per unit area for a 300nm SiO₂ thick device, V^{CNP} is the back-gate voltage value at the first and more positive CNP, and e is the electron charge. A normalization that considers the CNP at more positive voltage values as $n = 0 \text{ cm}^{-2}$ is adopted to better visualize the phenomenon (secondary peaks). As it will be explained later, such CNP presents the electrostatic conditions needed to neutralize charges at the graphene main channel. Figure 2(b) shows the dependence of the second CNP as a function of the electrode length d . Clearly, the second CNP is evident in devices with larger metallic electrodes. Such information is a strong evidence that charge is transferred to graphene underneath the contact, and, very likely, such graphene regions acquire a local charge density that is different from that of the graphene main channel. Moreover, both charge carrier type and density are tunable under interaction with H₂, corroborating with the hypothesis that the region underneath the contact is important for the interaction with H₂ molecules. Note that in this case, the measurements are performed from two neighbor terminals with similar electrodes length d , while the graphene geometry is kept fixed at $L = 1\mu\text{m}$ and $W = 3\mu\text{m}$. Hence, any contribution from the graphene area can be neglected.

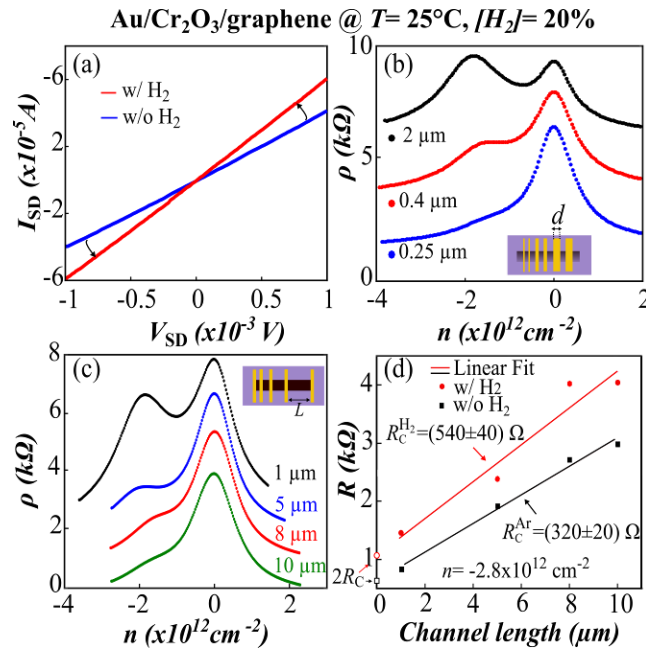


Figure 2. (a) $I_{SD} \times V_{SD}$ curves for a GFET with Au/Cr₂O₃ electrodes without (w/o) (blue) and with (w/) (red) H₂ exposure. Resistivity (ρ) as a function of carrier density (n) for different Au/Cr₂O₃ electrodes length, d (b), and graphene channel length, L (c) after 1h under H₂ exposure. In (a) and (b) the geometry is fixed at $L = 1 \mu\text{m}$ and $W = 3 \mu\text{m}$, while in (c) and (d) the electrodes are fabricated with $d = 1 \mu\text{m}$ and graphene width $W = 3 \mu\text{m}$. In figures (b) and (c) the curves are shifted to better visualize both CNPs. (d) Transfer length method resistance values measured for different graphene channel distances for the condition without (black) and with (red) gas exposure. All measurements presented in this figure are performed at room temperature ($T = 25^\circ\text{C}$) and $[H_2] = 20\%$.

We also investigate the relationship between the graphene channel L and the appearance of the second CNP in GFETs. In figure 2(c) we present data taken from GFETs with contacts of Au/Cr₂O₃, with several graphene channel lengths, and under $[H_2] = 20\%$ exposure at $T = 25^\circ\text{C}$. In all devices, the length of the contacts is kept fixed at $d = 1 \mu\text{m}$ and the measurements are performed from two neighbor terminals for different graphene lengths. From the $\rho \times n$ curves, we see that secondary CNPs are present mainly in short devices: GFETs with small graphene channel lengths. This data corroborates with the hypothesis that in shorter graphene main channels, the contribution of the graphene region underneath the electrodes are more significant [27,48,49]. Therefore, we can state that the ratio between the graphene and electrodes length is also important for the observation of multiples CNPs, as it would be expected [14,48].

A better presentation of the change of the contact resistance (R_C) of the devices before and after H_2 exposure is shown in figure 2(d). Here, we present data taken from the same device showed in figure 2(c), at a fixed value of $n = -2.8 \times 10^{12} \text{cm}^{-2}$ (left side of the CNP). The total resistance R scales linearly with L , and from the linear extrapolation of the resistance, we can estimate the intercept at $L = 0 \mu\text{m}$ which gives the sum of the R_C of both electrodes. Average contact resistance is then estimated as half the vertical intercept of the fitting line in Figure 2(d). Such values are presented in black, for devices without interaction with H_2 (R_C^{Ar}) and, in red, for devices under H_2 exposure ($R_C^{\text{H}_2}$). The fitted R_C values are $R_C^{\text{Ar}} = W. (320 \pm 20) \Omega \mu\text{m}$ and $R_C^{\text{H}_2} = W. (540 \pm 40) \Omega \mu\text{m}$, respectively. Therefore, one can notice that the GFETs exposed to H_2 depict higher contact resistance, indicating that R_C is affected by the hydrogen molecules, $R_C^{\text{H}_2}/R_C^{\text{Ar}} \approx 69\%$. We also show in the Supporting Information the analysis of contact resistance for values at the right side of the CNP in figure 2(c). One can note that a similar behavior is observed with a change in R_C and a decrease of the contact resistance of about $R_C^{\text{H}_2}/R_C^{\text{Ar}} \approx 93\%$ after hydrogen exposure. These results suggest that H_2 molecules can significantly change the metal-graphene interface potential. For instance, we believe that such molecules modify the p-n junctions at the metal-graphene regions, therefore changing the preferential scattering mechanisms (asymmetry in the transfer curves), as previously discussed. In other words, changes in the doping level at the metal-graphene interface define the preferential scattering for either holes or electrons, modifying then the contact resistance measured. Consequently, this phenomenon explains the increase observed for $R_C^{\text{H}_2}$ for the left side of CNP (hole-branch) and decrease for the right (electron-branch) side.

Next, we present in more detail the time dependence of the multiple CNPs for the GFETs with $\text{Au}/\text{Cr}_2\text{O}_3$ electrodes. Figure 3(a) shows the evolution of the second CNP as function of the exposure time to $[H_2] = 20\%$ at $T = 200^\circ\text{C}$ for a device fabricated with $d = 1 \mu\text{m}$. Initially, under an Argon atmosphere (without H_2), the RxV_G curve depicts only one CNP at $V_G^{\text{ch}} = -7.6\text{V}$, which

we label it as the CNP position for the graphene channel. However, as soon as there is H₂ inside the chamber (adsorption), the electron charge transfer takes place (V_G^{ch} shifts to more negative values $V_G^{ch} = -13.7V$) and a second CNP emerges, stabilizing at around 30min under gas exposure at $V_G^{cont} = -37V$, which we label as the CNP position for the graphene underneath the electrodes. When we turn off the H₂ gas (desorption) the system returns to the initial stage, with a single CNP (figure 3(b)). It is important to stress that the interaction of the device with molecular hydrogen is completely reversible. For measurements under $[H_2] = 20\%$ the desorption time is larger than 1.5h. We also need to emphasize that the desorption depends on the length d of the electrodes: decreasing its length also decreases the desorption time. For instance, the desorption time drops from 5h for a length of $d = 2\mu m$ to 0.5h for $d = 0.5\mu m$. This effect is consistent with the diffusion of H₂ molecules in between the graphene sheet and the electrodes, indicating that the trapped molecules can easily escape from narrower metallic contacts. Also, the saturation time interestingly decreases for contacts with longer lengths. For $d = 2\mu m$, for example, the saturation time is about 3min, while for $d = 0.5\mu m$ it is 8min. Such non-expected behavior is still not clear to us and this process is under new studies. Manipulation and control over the device time evolution is crucial for providing a faster route to detect molecular hydrogen using metal-type engineering in GFETs.

Even though the data presented in figures 3(a) and 3(b) correspond to a temperature $T = 200^\circ C$, the same behavior occurs for temperatures ranging from $T = 25^\circ C$ up to $T = 200^\circ C$. For instance, figure 3(c) shows $R \times n$ curves for all temperatures analyzed after 1h under $[H_2] = 20\%$ exposure. One can note that the appearance of the second CNP does not depend on the temperature: even at $T = 25^\circ C$ there is the formation of the second CNP. The fact that the second CNP can be observed at room temperature, but with a very small charge transfer process with H₂ exposure (see Supplementary Information), would indicate that both phenomena are in fact decoupled from each other, having different origins as we will discuss later. Moreover, from figure 3(c) it is possible to observe an increase in the splitting between the CNPs as the

temperature increases, which is also presented in more detail in figure 3(d). In this figure, we show the Fermi energy variation (ΔE_{Fermi}) calculated between both CNPs as a function of temperature. In this case, the Fermi energy variation is defined by $\Delta E_{Fermi} = \hbar v_F \sqrt{\pi |\Delta n|}$, where $\hbar = 6.58 \times 10^{-16} eV.s$ is the Planck's constant ($h/2\pi$), the Fermi velocity is given by $v_F = 1 \times 10^6 m/s$ and $|\Delta n|$ is the difference of the amount of charge density in between both CNPs [31,47]. In this figure, one can note that the splitting in energy increases up to $T = 150^\circ C$ and decreases afterwards for $T = 200^\circ C$. The origin for such decrease is still unclear at the moment. Such results indicate that the interaction at the metal-graphene interface is also favored at higher temperatures, showing that modifications at the metal-graphene interface by H_2 molecules are thermally activated. Additionally, the splitting between both CNPs is also dependent on the H_2 concentration. In figure 3(e) we present the $R \times n$ curves for all concentrations analyzed (from $[H_2] = 0.5\%$ up to $[H_2] = 50\%$) and after 1h under H_2 exposure at $T = 200^\circ C$. This result shows that both the intensity of the second CNP and the splitting between both CNPs depend on the H_2 concentration, see figure 3(f). This indicates that the amount of H_2 at the interface is determinant for the definition of the doping level at the region underneath the electrodes.

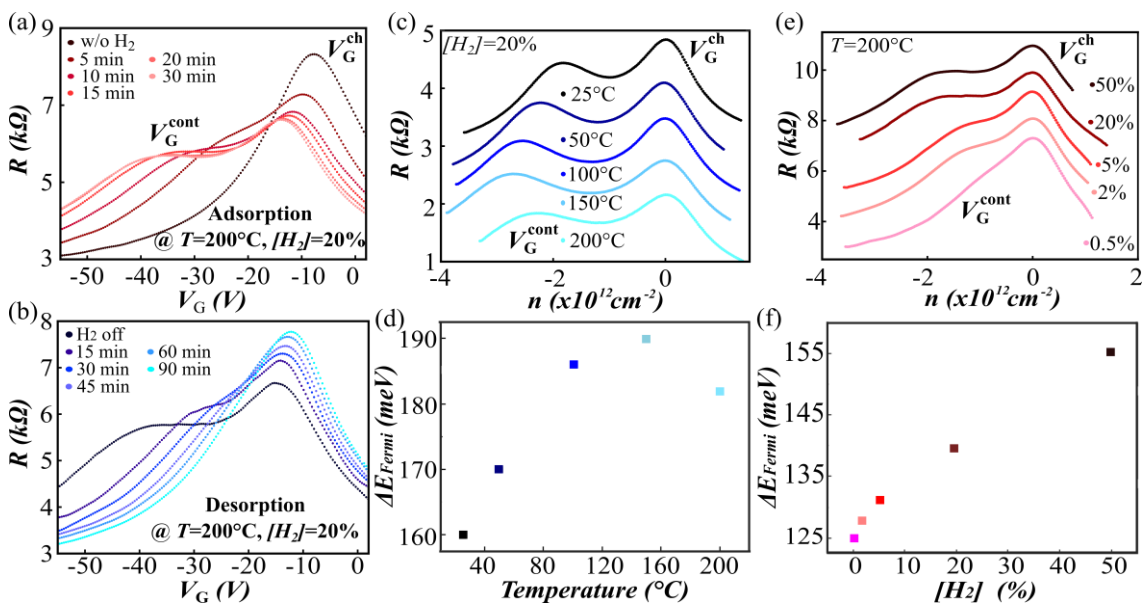


Figure 3. $R \times V_G$ curves for different time of exposure to $[H_2]=20\%$ in argon during adsorption (a) and desorption (b) processes at $T=200^\circ C$. (c) $R \times n$ for different temperatures, which the measurements are

obtained after 1h under exposure to $[H_2]=20\%$. (d) Variation of Fermi energy (ΔE_{Fermi}) between both CNPs as a function of temperature. (e) $R \times n$ for different $[H_2]$, where the measurements are obtained after 1h at $T=200^\circ\text{C}$. (f) $\Delta E_{Fermi} \times [H_2]$ at $T=200^\circ\text{C}$. All the measurements presented in this figure are performed on a GFET fabricated with Au/Cr₂O₃ electrodes and contact length of $d=1\mu\text{m}$.

Now, it is important to stress that apart from a double-gate structure that enables setting of the density of charges at different regions of the graphene channel independently, all the other processes that create a double-CNP are irreversible [21,28,31,43,47,49]. In our case, the formation of the second CNP is totally controlled and reversible in devices fabricated with a 1nm thick layer of Cr₂O₃, and under hydrogen exposure. However, if the GFETs are fabricated with 5nm or 10nm of Cr₂O₃, the second CNP is presented even before H₂ gas exposure, but are also tunable under H₂ interaction (see the Supporting Information). In such conditions, when the devices are exposed to H₂ there is a shift of both CNPs towards more negative gate values, indicating that both regions (graphene main channel and graphene underneath the contacts) accept electrons. We shall also comment that GFETs with thick layers of Cr₂O₃ are extremely unstable at high temperatures whereas devices fabricated with 1nm Cr₂O₃ thick are very stable.

We will now address possible explanations for the phenomenology associated to H₂ doping. Let us first consider possible physical mechanisms for the n-doping action of H₂ molecules on an Au-graphene interface, without the presence of either Cr or Cr₂O₃, as evidenced by the results of figure 1(a). Our discussion will be based on existing theoretical first-principles results on the literature, as well as on previous experimental evidence. A detailed first-principles study of electronic and structural properties of interfaces between graphene and the 111 surfaces of Al, Ag, Cu, Au, and Pt has been performed in the works of Giovannetti *et al.*, and Khomyakov *et al.* [16,50] The first-principles results show that the shift of the CNP of graphene with respect to the Fermi level, ΔE_F , is an increasing monotonic function of the metal-graphene distance for all interfaces. For the Au-graphene case at the equilibrium distance, the calculation shows graphene as p-type doped, with ΔE_F of 0.19eV. Therefore, an increase of this distance due to the

This is the authors' version (pre peer-review) of the manuscript: C. L. Pereira et al 2D Materials <https://doi.org/10.1088/2053-1583/ab0b23>

That has been published in its final form: <https://iopscience.iop.org/article/10.1088/2053-1583/ab0b23/meta>

presence of an H₂ interlayer would result in additional p-doping, and not n-doping, from geometrical reasons alone. The calculations also show a positive and monotonic dependence of ΔE_F with $W_M - W_G$, where W_M and W_G are the work functions of the isolated metal surface and graphene, respectively. Among the investigated systems, the ones closest to the neutrality condition ($\Delta E_F = 0$) are Au and Cu, with Au being slightly p-dopant ($\Delta E_F = 0.19\text{eV}$) and Cu being slightly n-dopant ($\Delta E_F = -0.17\text{eV}$). The calculated work functions W_M of the Au and Cu surface are respectively 5.54eV and 5.22eV. From our measured n-type carrier density of the order of $2 \times 10^{12}\text{cm}^{-2}$ under hydrogen exposure, we can estimate, from the electronic density of states of graphene, that $\Delta E_F = -0.16\text{eV}$, very similar to the calculated value for Cu. We therefore estimate that the net action of H₂ exposure is to reduce the work function W_M of Au by order of 0.3eV and consequently transform the graphene doping from p-type to n-type.

Are there known experiments involving H₂ adsorption that could lead to reductions of the Au surface work function W_M by tens of an eV? The answer is “yes” for Au-TiO₂-Ti diodes used as high sensitivity H₂ sensors [51]. In this work, the Ohmic behavior of the Au-TiO₂ junction in hydrogen atmosphere was associated to a reduction of the Au surface work function by several tens of an eV. An additional experimental information on the charge transfer between Au and H₂ has been recently reported [52]. These experiments reported a negative charge transfer from Au nanoparticles to adsorbed H₂ at ambient conditions, such that these nanoparticles become positively charged. This last information can, in principle, provide a possible mechanism for a negative charge transfer from non-planar regions of Au to graphene in the presence of adsorbed H₂.

Now, let us discuss the formation of the second CNP based on the literature. Previous works [17,43,46,49] discussed the observation of multiple CNPs when the Fermi level pinning induced by the electrodes is weak. Hence the graphene underneath the contact can be modulated by gate bias, resulting in changes of the charge density between both regions. Moreover, at the conditions of weak metal-graphene interaction, the conical points in the graphene band structure

are preserved, but charge transfer to or from the metallic electrodes can take place, modulating then the Fermi level at the region underneath the contacts [16,50]. Other works also demonstrate that the formation of oxide layer in between graphene and the electrodes could be the reason of multiple CNPs [27,48,49]. In our present case, the second CNP appears with the presence of chromium oxide and under H₂ exposure. In an experimental work on chromium oxide gas sensors, Miremadi *et al.*[53] observed the reduction of the conductivity of p-type sensors as a function of hydrogen concentration. This n-type dopant action of H₂ was associated with the reduction of Cr⁴⁺ to Cr³⁺ at the oxide surface. Therefore, we might be facing two distinct mechanisms for H₂-induced n-doping, one associated to Au-graphene (as discussed in the preceding paragraphs) and the other associated to chromium oxide-graphene. The latter H₂-doping mechanism has been proposed to involve the modification of the oxide surface [53]. We suggest that this mechanism might also result in the decoupling of the electron states of graphene from those of the oxide contact regions. Such decoupling has been considered a necessary ingredient for the appearance of two CNPs in RxV_G curves of GFETs with Ni contacts due to the oxidation of Ni at contact regions [27,48,49], and such RxV_G curves are similar to the one observed in figure 1(d) upon H₂ exposure, suggesting a similar physical origin.

Finally, figure 4 illustrates a phenomenological model for the different metal/graphene heterojunctions studied. Figure 4(a) shows that effect of the molecular hydrogen when only Au metallic contacts are used. In this case, the RxV_G curve shows only one CNP and the asymmetry generated by the p-type doping induced by the Au-electrodes and pinning of the graphene work function by the metal [16,17,45]. In this case the Fermi energy (E_F) level for the region underneath the contact remains fixed due to the charge density pinning, while the E_F for the channel region can be tunable by the gate bias. However, we suggest that the H₂ molecules modify the interface potential by interacting with Au interface reducing its work function and causing the observed n-type doping effect. Now, figure 4(b) depicts the case of GFETs with Au/Cr electrodes without H₂ exposure, where the RxV_G curve also shows a single CNP and asymmetry induced by the

This is the authors' version (pre peer-review) of the manuscript: C. L. Pereira et al 2D Materials
<https://doi.org/10.1088/2053-1583/ab0b23>

That has been published in its final form: <https://iopscience.iop.org/article/10.1088/2053-1583/ab0b23/meta>

electrodes and pinning of the graphene work function [16,17,45]. Moreover, similar to the case of pristine gold, the E_F for the region underneath the contact remains fixed, while the E_F for the graphene channel can be tunable by the gate bias. In this case, when the hydrogen is turned on, the RxV_G curve presents a single CNP, and a subtle n-type doping, as illustrated in figure 4(b). Nevertheless, solely for GFETs with Au/Cr₂O₃ electrodes, the RxV_G curves present two CNPs when the hydrogen is turned on, as we illustrate in figure 4(c). Such observation can be associated to the decoupling of the work functions between the metal and graphene that occurs induced by the presence of H₂ molecules at the metal-graphene interface. In the latter case, the E_F of both regions are modulated by the gate bias, and if both regions exhibit different doping levels, the RxV_G curve shows double-CNP, one of them originated from the minimum of density of states in the graphene channel and the other coming from the graphene at the contact region.

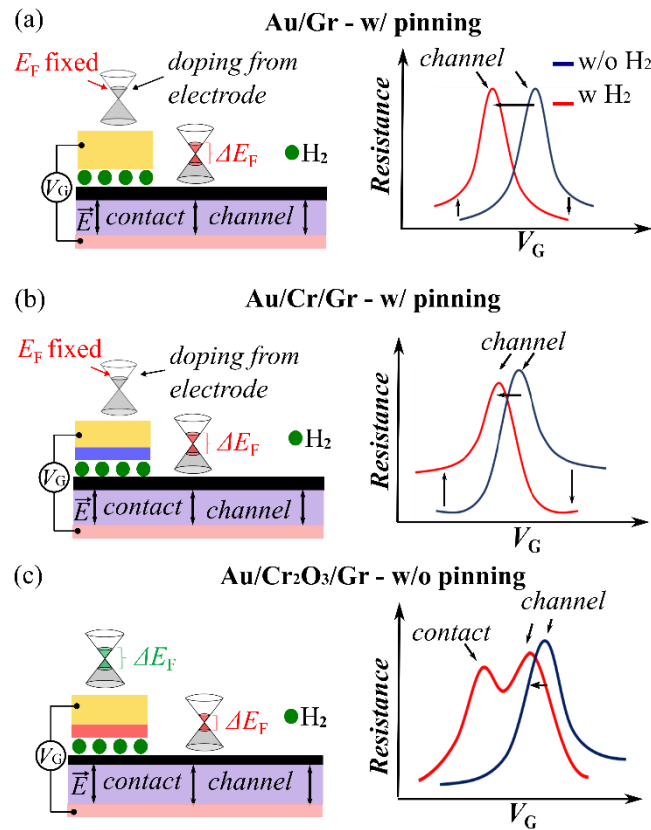


Figure 4. (a) A schematic of the graphene device with hydrogen exposure for GFETs with Au metallic electrodes. The band diagram on the contact region indicates the Fermi level pinning (E_F fixed) induced by the metallic electrode, and the band diagram on channel region shows the E_F modulation by the V_G application. The RxV_G curve presents only one CNP associated solely with the graphene channel. (b) A schematic of the graphene device with gas exposure for GFETs with Au/Cr metallic electrodes. The RxV_G curves present also the Fermi level pinning (E_F fixed) before and after H_2 exposure. (c) A schematic of the graphene device with gas exposure for GFETs with Au/ Cr_2O_3 metallic electrodes. The band diagram of the graphene underneath the contact and at the channel regions show the E_F modulation by the gate bias, demonstrating now the existence of double-CNP in the RxV_G curve.

4 – CONCLUSION

In summary, we have investigated the formation of multiple charge neutrality points induced in graphene devices by molecular hydrogen exposure. Our findings demonstrate that the observation of the “M-shape” on the RxV_G curves obtained by using thin layers of chromium oxide as metal-type electrodes is not solely dependent on the graphene channel and electrodes size, but also on hydrogen concentration and the temperature at which the interaction occurs.

This is the authors' version (pre peer-review) of the manuscript: C. L. Pereira et al 2D Materials <https://doi.org/10.1088/2053-1583/ab0b23>

That has been published in its final form: <https://iopscience.iop.org/article/10.1088/2053-1583/ab0b23/meta>

Moreover, our study confirms that the formation of the second CNP is totally reversible and indicates that after H₂ exposure the graphene regions underneath the electrodes can be modulated by the gate bias. Therefore, our results are valuable for two reasons: first, for a better understanding of the metal-graphene interface and the formation of multiple CNPs; second, it shows that the electrode engineering can be used to improve the hydrogen detection using non-functionalized graphene devices.

ACKNOWLEDGEMENTS

This work was supported by CAPES, Fapemig (Rede 2D), CNPq and INCT/Nanomateriais de Carbono. The authors are thankful to Lab Nano at UFMG for allowing the use of atomic force microscopy and Laboratório de Cristalografia at UFMG for allowing the use of X-ray excited photoelectron spectroscopy. The authors also acknowledge I. S. L. Antoniazzi for the AFM measurements and V. Ornelas for improvements in the gas sensing system employed in this work.

REFERENCES

- [1] Novoselov K S, Geim A K, Morozov S V, Jiang D, Zhang Y, Dubonos S V, Grigorieva I V and Firsov A A 2004 *Science* **306** 666–9
- [2] Novoselov K S, Fal'Ko V I, Colombo L, Gellert P R, Schwab M G and Kim K 2012 *Nature* **490** 192–200
- [3] Ferrari A C et al *Nanoscale* **7** 4598–810
- [4] Castro Neto A H, Peres N M R, Novoselov K S, Geim A K and Guinea F 2009 *Reviews of Modern Physics* **81** 109–62
- [5] Schwierz F 2010 Graphene transistors *Nature Nanotechnology* **5** 487–96
- [6] Zhan B, Li C, Yang J, Jenkins G, Huang W and Dong X 2014 *Small* **10** 4042–65
- [7] Yan F, Zhang M and Li J 2014 *Advanced Healthcare Materials* **3** 313–31

- [8] Wang F, Zhang Y, Tian C, Girit C, Zettl A, Crommie M and Shen Y R 2008 *Science* **320** 206–9
- [9] Li J, Niu L, Zheng Z and Yan F 2014 *Advanced Materials* **26** 5239–73
- [10] Bonaccorso F, Sun Z, Hasan T and Ferrari A C 2010 *Nature Photonics* **4** 611–22
- [11] Barcelos I D, Cadore A R, Alencar A B, Maia F C B, Mania E, Oliveira R F, Bufon C C B, Malachias Â, Freitas R O, Moreira R L and Chacham H 2018 *ACS Photonics* **5** 1912–18
- [12] Cadore A R, Mania E, Watanabe K, Taniguchi T, Lacerda R G and Campos L C 2016 *Applied Physics Letters* **108** 033109
- [13] Ardito F M, Mendes-De-Sá T G, Cadore A R, Gomes P F, Mafra D L, Barcelos I D, Lacerda R G, Iikawa F and Granado E 2018 *Physical Review B* **97** 035419
- [14] Nouchi R 2017 *Nanotechnology* **28** 134003
- [15] Barraza-Lopez S, Vanević M, Kindermann M and Chou M Y 2010 *Physical Review Letters* **104** 076807
- [16] Giovannetti G, Khomyakov P A, Brocks G, Karpan V M, Van Den Brink J and Kelly P J 2008 *Physical Review Letters* **101** 026803
- [17] Song S M and Cho B J 2013 *Carbon letters* **14** 162–70
- [18] Song S M, Park J K, Sul O J and Cho B J 2012 *Nano Letters* **12** 3887–92
- [19] Low T, Hong S, Appenzeller J, Datta S and Lundstrom M S 2009 *IEEE Transactions on Electron Devices* **56** 1292–9
- [20] Huard B, Stander N, Sulpizio J A and Goldhaber-Gordon D 2008 *Physical Review B - Condensed Matter and Materials Physics* **78** 121402
- [21] Peng S, Jin Z, Zhang D, Shi J, Niu J, Huang X, Yao Y, Zhang Y and Yu G 2018 *Advanced Electronic Materials* **4** 1800158
- [22] Wang L, Meric I, Huang P Y, Gao Q, Gao Y, Tran H, Taniguchi T, Watanabe K, Campos L M, Muller D A, Guo J, Kim P, Hone J, Shepard K L and Dean C R 2013 *Science* **342** 614–7
- [23] Cadore A R, Mania E, De Morais E A, Watanabe K, Taniguchi T, Lacerda R G and Campos L C 2016 *Applied Physics Letters* **109** 033109

- [24] Geim, A. K.; Novoselov K S 2007 *Nature Materials* **6** 183–91
- [25] Park M, Yun Y J, Lee M, Jeong D H, Jun Y, Park Y W and Kim B H 2015 *AIP Advances* **5** 017120
- [26] Brenner K and Murali R 2010 *Applied Physics Letters* **96** 063104
- [27] Nouchi R and Tanigaki K 2015 *Applied Physics Letters* **106** 083107
- [28] Sun Y, Xie D, Zhang C, Li X, Xu J, Sun M, Teng C, Li X and Zhu H 2017 *Journal of Applied Physics* **121** 134305
- [29] Yu X, Shen Y, Liu T, Wu T and Jie Wang Q 2015 *Scientific Reports* **5** 1–8
- [30] Iqbal M Z, Anwar N, Siddique S, Iqbal M W and Hussain T 2017 *Optical Materials* **69** 254–8
- [31] Zhang C, Xie D, Xu J-L, Li X-M, Sun Y-L, Dai R-X, Li X and Zhu H-W 2015 *Journal of Applied Physics* **118** 144301
- [32] Wang J X, Huang Q Q, Wu C L, Wei Z J, Xuan N N, Sun Z Z, Fu Y Y and Huang R 2015 *RSC Advances* **5** 80496–500
- [33] Williams J R, DiCarlo L and Marcus C M 2007 *Science* **317** 638–41
- [34] Huard B, Sulpizio J A, Stander N, Todd K, Yang B and Goldhaber-Gordon D 2007 *Physical Review Letters* **98** 236803
- [35] Campos L C, Young A F, Surakitbovorn K, Watanabe K, Taniguchi T and Jarillo-Herrero P 2012 *Nature Communications* **3** 1236–9
- [36] Silvestre I, De Morais E A, Melo A O, Campos L C, Goncalves A M B, Cadore A R, Ferlauto A S, Chacham H, Mazzoni M S C and Lacerda R G 2013 *ACS Nano* **7** 6597–604
- [37] Cadore A R, Mania E, Alencar A B, Rezende N P, de Oliveira S, Watanabe K, Taniguchi T, Chacham H, Campos L C and Lacerda R G 2018 *Sensors and Actuators B: Chemical* **266** 438–46
- [38] Rezende N P, Cadore A R, Gadelha A C, Pereira C L, Ornelas V, Watanabe K, Taniguchi T, Ferlauto A S, Malachias A, Campos L C and Lacerda R G 2018 *Advanced Electronic Materials* **1800591** 1-8
- [39] Romero H E, Shen N, Joshi P, Gutierrez H R, Tadigadapa S a., Sofo J O and Eklund P C

2008 *ACS Nano* **2** 2037–44

- [40] Kim B H, Hong S J, Baek S J, Jeong H Y, Park N, Lee M, Lee S W, Park M, Chu S W, Shin H S, Lim J, Lee J C, Jun Y and Park Y W 2012 *Scientific Reports* **2** 1–6
- [41] Hong S J, Park M, Kang H, Lee M, Soler-Delgado D, Shin D S, Kim K H, Kubatkin S, Jeong D H, Park Y W and Kim B H 2015 *Applied Physics Letters* **106** 142110
- [42] Chiu H Y, Perebeinos V, Lin Y M and Avouris P 2010 *Nano Letters* **10** 4634–9
- [43] Bartolomeo A Di, Giubileo F, Santandrea S, Romeo F, Citro R, Schroeder T and Lupina G 2011 *Nanotechnology* **22** 275702
- [44] Xia F, Perebeinos V, Lin Y M, Wu Y and Avouris P 2011 *Nature Nanotechnology* **6** 179–84
- [45] Peng S, Jin Z, Zhang D, Shi J, Zhang Y and Yu G 2017 *Nanoscale* **9** 9520–8
- [46] Karnatak P, Sai T P, Goswami S, Ghatak S, Kaushal S and Ghosh A 2016 *Nature Communications* **7** 1–8
- [47] Feng T, Xie D, Xu J, Zhao H, Li G, Ren T and Zhu H 2014 *Carbon* **79** 363–8
- [48] Nouchi R and Tanigaki K 2014 *Applied Physics Letters* **105** 033112
- [49] Nouchi R and Tanigaki K 2010 *Applied Physics Letters* **96** 253503
- [50] Khomyakov P A, Giovannetti G, Rusu P C, Brocks G, Van Den Brink J and Kelly P J 2009 *Physical Review B - Condensed Matter and Materials Physics* **79** 195425
- [51] Rahbarpour S and Hossein-Babaei F 2011 *Key Engineering Materials* **495** 289–93
- [52] Watkins W L and Borensztein Y 2017 *Phys. Chem. Chem. Phys.* **19** 27397–405
- [53] Miremedi B K, Singh R C, Chen Z, Roy Morrison S and Colbow K 1994 *Sensors and Actuators B: Chemical* **21** 1–4

Supporting Information

Reversible doping of graphene field effect transistors by molecular hydrogen: the role of the metal/graphene interface

C. L. Pereira^{1,2}, A. R. Cadore^{1,2}, N. P. Rezende¹, A. Gadelha¹, E. A. Soares¹, H. Chacham¹, L. C. Campos¹, R. G. Lacerda^{1,*}

¹*Departamento de Física, Universidade Federal de Minas Gerais, Belo Horizonte, 30123-970, Brasil*

²*These authors contributed equally to this work.*

**Electronic mail: rlacerda@fisica.ufmg.br*

1 – Identification of the chromium oxide layer (Cr₂O₃) by Atomic force microscopy (AFM) and X-ray excited photoelectron spectroscopy (XPS)

The chromium oxide layer is obtained using a thermal evaporation chamber as the following: immediately after chromium (Cr) deposition (~1nm), performed usually at pressures around 2×10^{-6} Torr, the thermal evaporator chamber is opened to atmospheric pressure for 30min (to promote the Cr oxidation), then pumped back down to 2×10^{-6} Torr, before the gold deposition on the top of it. However, to identify the formation of the oxide layer and its stoichiometry the final top gold layer was not deposited. Then, the oxidized Cr film was characterized by Atomic Force Microscope (AFM) and x-ray excited photoelectron spectroscopy (XPS). Figure S1(a) shows the topography image of the chromium oxide layer thermally evaporated on SiO₂/Si obtained by AFM. As can be seen the oxidized Cr layer has a rough-like structure with about 2 nm of thickness. This kind of morphology is expected for very thin layer films deposited by thermal evaporation.

Figure S1(b) shows the XPS analysis of chromium oxide. With this result, we can infer the stoichiometry of the oxide formed under ambient conditions. The long range energy spectrum shows photoelectron peaks that can be assign to Cr, O, C and Si. From the high resolution spectrum in the Cr 2p region (inset of Fig.S1(b)), we determine that

the binding energy of the Cr 2p^{3/2} peak is 576.4 eV and that the spin orbit splitting of the 2p level is 9.7 eV. The reported values of these quantities in the literature for Cr₂O₃ are 576.9 eV and 9.8 eV, respectively [1]. Therefore, we can conclude the formation of a Cr₂O₃ layer in our sample.

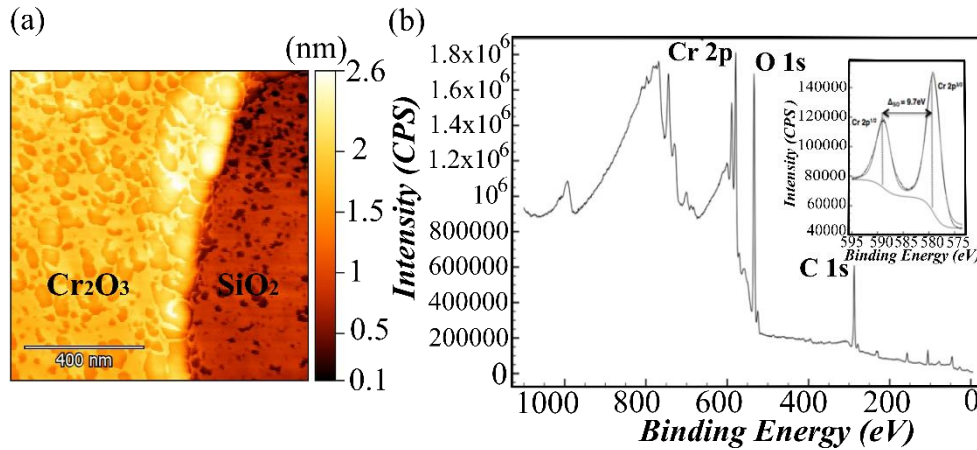


Figure S1. (a) Atomic force microscopy of Cr₂O₃ film (1nm). (b) X-ray excited photoelectron spectroscopy after the oxidation of 1nm of chromium.

2 – Two-probe measurements in devices with Hall bar configuration

As described in the main manuscript text, graphene devices that are fabricated in a Hall bar configuration and exposed to H₂ gas do not present neither charge transfer nor the formation of the double-CNP. However, if the same device is measured in a two-probe configuration, both features can be observed. For instance, Figure S3(a) shows the two-probe RxV_G measurements between the more distant contacts ($L=15\mu\text{m}$), while Figure S3(b) exhibits for the nearest terminals ($L = 7\mu\text{m}$). In the primer case, the emergence of second CNP under H₂ exposure is not evident but becomes clear for the shorter channel where a second CNP can be seen at $V_G^{ch} = -25V$. Note that such results are in total agreement with Figure 2(d) in the main text, where we described the dependence of channel length with the observation of two CNPs.

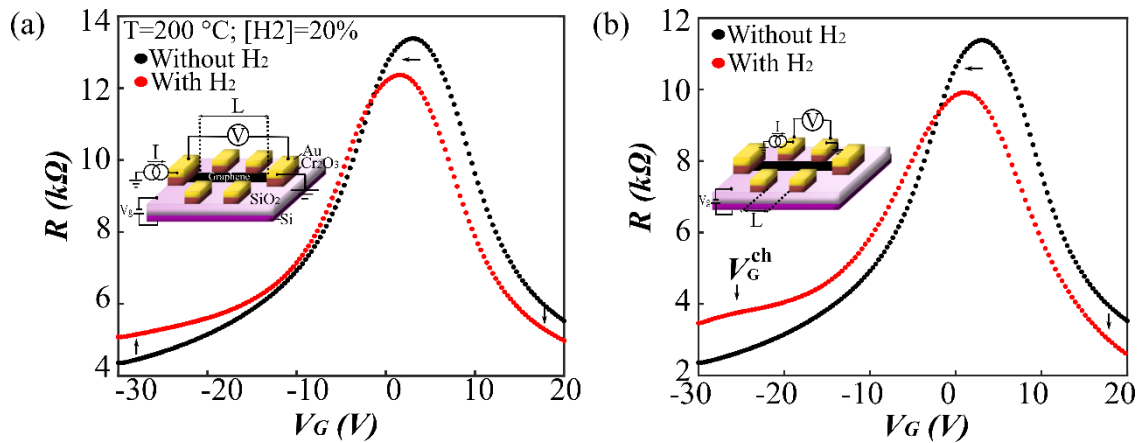


Figure S3. Two-probe $R \times V_G$ curves for a GFET fabricated in Hall bar geometry with Au/Cr₂O₃ electrodes between the (a) farthest terminals ($L=15\mu\text{m}$) and (b) closest ones ($L=7\mu\text{m}$). Measurements presented in this figure are performed at $T=200^\circ\text{C}$ and the data under $[H_2]=20\%$ (red curves) are performed after 1h of gas exposure, while the black curves are measurements in pure argon, before turning on the molecular hydrogen.

4- Hysteresis of the GFETs with different metal-type electrodes

Figure S4 presents an investigation of the double-CNP by measuring the hysteresis of the GFETs for all metal-type electrodes. The left panels present the V_G forward scan (indicated by the blue arrows) with (red) and without (black) H₂ exposure, while the right panels present the same case for V_G backward scan (indicated by the green arrows). The measurements show that the $R \times V_G$ curves before and after exposure to hydrogen for all types of metal electrodes studied in this work have the same shape, regardless of the direction of the sweep of the applied potential window. This means that the observed effects due to hydrogen, both n-type doping and the appearance of the second peak, are not associated with trapped charges at the graphene-substrate interface [2,3].

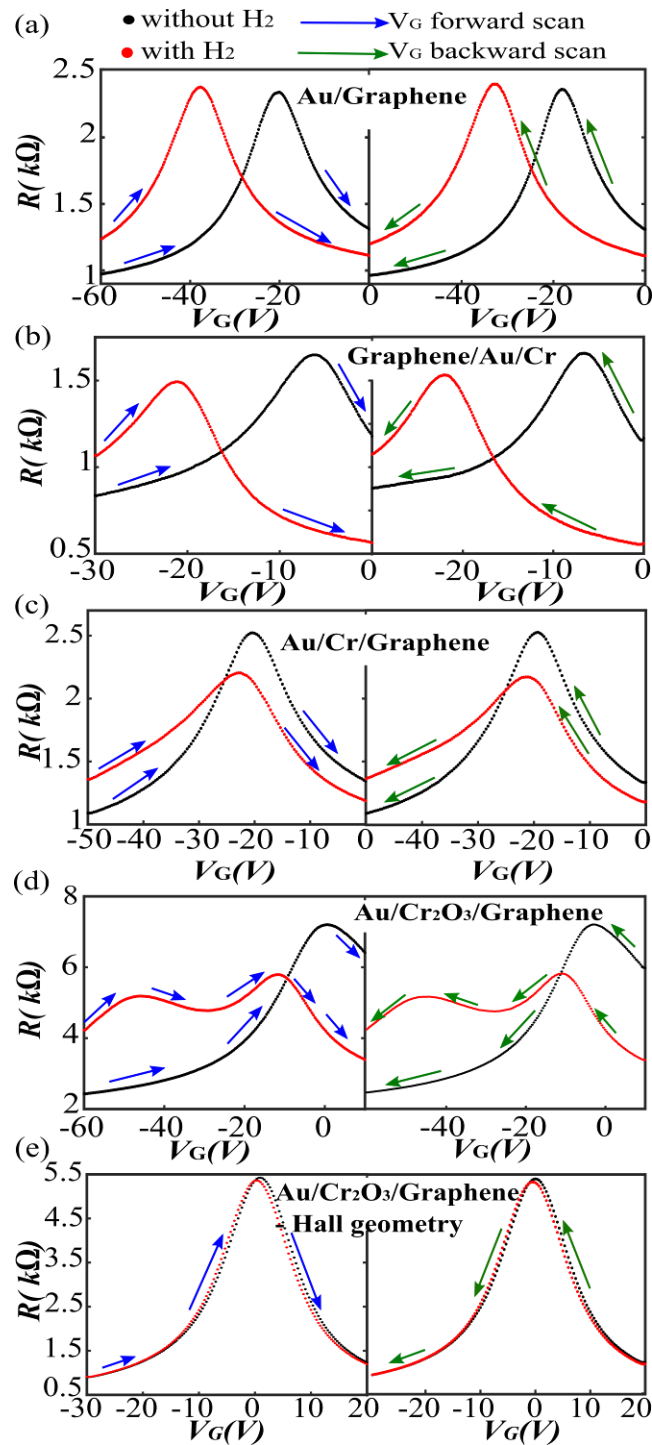


Figure S4. RxV_G curves with (red) and without (black) H₂ exposure for GFETs with pure Au (a), Cr/Au (b), Au/Cr (c), Au/Cr₂O₃ (d) electrodes. While in (e) is the GFET in hall geometry with Au/Cr₂O₃ electrodes.

5 – $I_{SD} \times V_{SD}$ curves for different configurations of metal-types

Figure S5 shows $I_{SD} \times V_{SD}$ curves of all the metal-type configurations used in our work. In all the curves, for each contact geometry (represented in the insets), an Ohmic behavior is observed before (blue) and after (red) exposure to hydrogen. One can note that the linear relation between $I_{SD} \times V_{SD}$ of the device is not affected by the molecules, while the small variation in the current values is associated with the charge transfer to graphene channel.

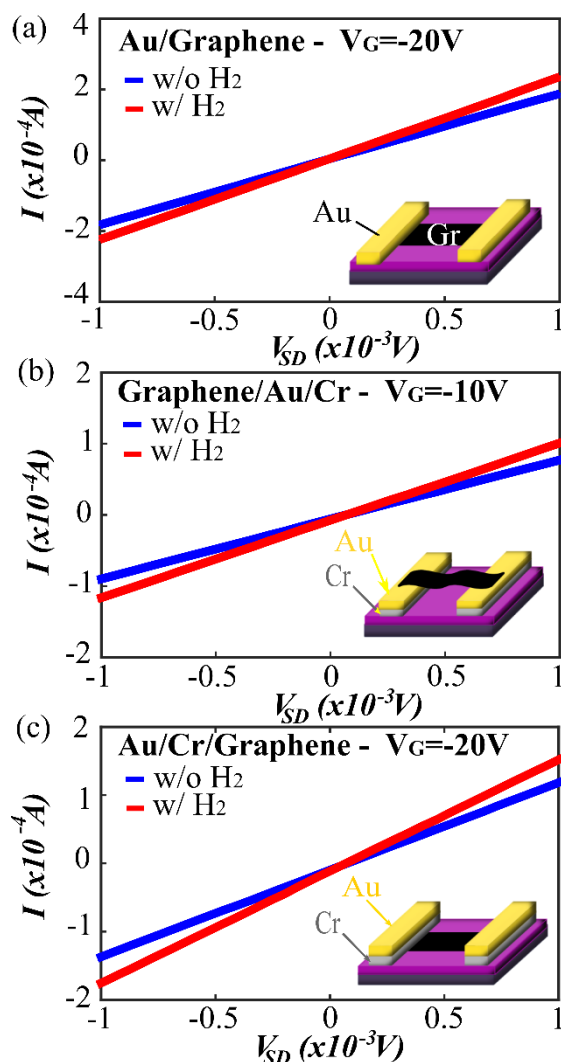


Figure S5. $I_{SD} \times V_{SD}$ curves without (w/o) (blue) and with (w/) (red) H₂ exposure for a GFET with (a) Au, (b) Cr/Au and (c) Au/Cr.

In more detail, Figure S6 shows the $I_{SD} \times V_{SD}$ curves as a function of V_G for Au/Cr₂O₃/graphene devices, where the Ohmic behavior appears for all V_G values. Figure S6(a) shows a single value of V_G in which the current decays and subsequently increases, indicating a single CNP before gas exposure. This aspect can be clearly seen in the $R \times V_G$ curve presented in the inset of the same figure. However, Figure S6(b) shows two distinct values of V_G at which the current decreases, indicating the formation of two CNPs after the exposure (see inset of the same figure).

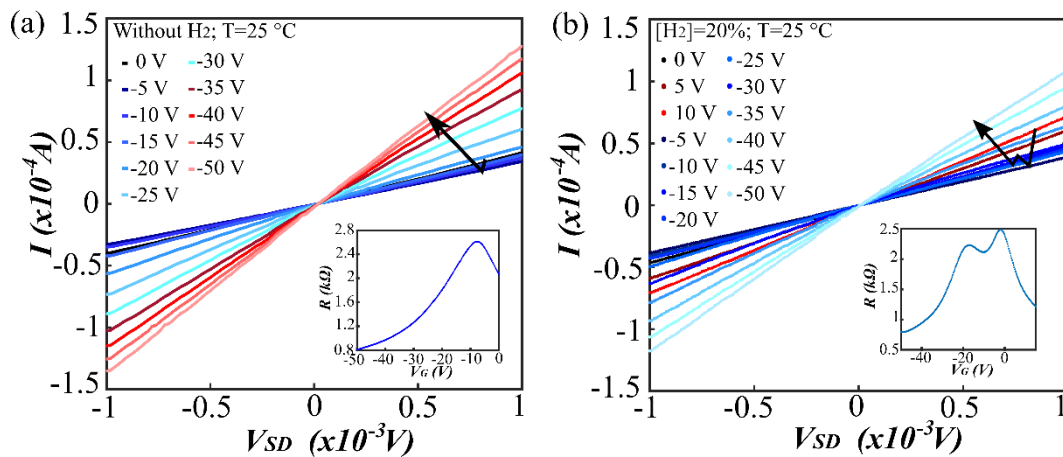


Figure S6. (a) $I_{SD} \times V_{SD}$ curves w/o H₂ exposure for a GFET with Au/Cr₂O₃ electrodes. The inset shows the two-probe $R \times V_G$ curve at the same conditions. (b) $I_{SD} \times V_{SD}$ curves under H₂ exposure for the same device. The inset brings the $R \times V_G$ curve at the same conditions. The measurements were carried out 1h after hydrogen exposure. All the measurements presented in this figure were performed at $T=25^\circ\text{C}$ and $[\text{H}_2]=20\%$.

6 – Electron charge transfer for different graphene devices at room temperature

Figure S7 shows the $R \times V_G$ curves for the same conditions of temperature (25°C) and $[\text{H}_2]=20\%$, for the different metal-types electrodes used in this work. The $R \times V_G$ curves for all devices do not present any significant shift for more negative values of gate voltage. For instance, one can note that the position of the CNP which is associated with the graphene slightly shifts to negative values but no larger than $\Delta V_G^{ch} = 3\text{V}$, demonstrating a small charge transfer at room temperature. However, as mentioned on

the text, such shift can be as large as $\Delta V_G^{ch} = 20V$ at $T=200\text{ }^\circ\text{C}$, demonstrating that the charge transfer is a thermally activated process.

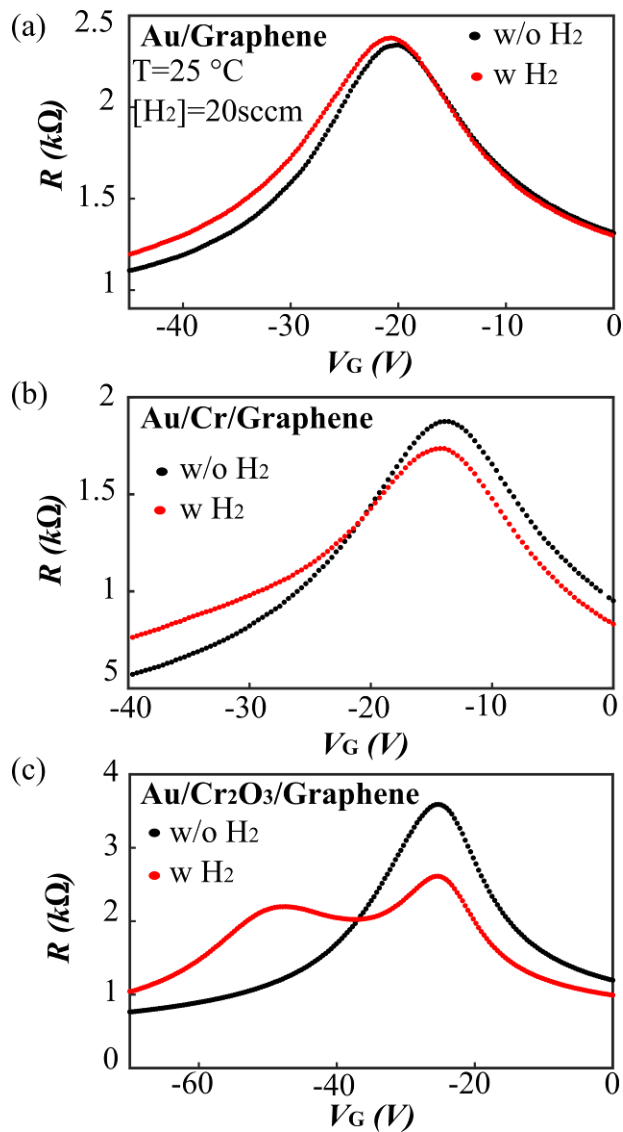


Figure S7. R vs V_G curves at room temperature (25°C) and $[H_2]=20\%$. The devices are prepared with (a) Au electrodes, (b) Au/Cr electrodes and (c) Au/Cr₂O₃ electrodes.

7 – Graphene devices prepared with a different Cr₂O₃ thickness

As described in the main text, all the samples measured using 1nm of Cr₂O₃ do not show any additional CNP after fabrication and without H₂ exposure. However, devices were also fabricated using a thicker oxide layer, such as 5nm and 10nm Cr₂O₃ but with a similar top gold layer thickness (30nm), forming the Au/Cr₂O₃/graphene/SiO₂/Si structures. The $R \times V_G$ curves of these new devices always present two CNP without any H₂ exposure at ambient temperature and Argon atmosphere, as shown in Figure S8. For both Cr₂O₃ thickness tested, the curves present immediately the “M-shaped” form, independently of the environment. For such devices is not clear which CNP is related to the graphene channel region or underneath the electrodes. However, we consider that such oxide thicknesses are enough to induce the decoupling between both work functions, as observed in previous works [4,5]. Therefore, comparing the results for thin oxide layers as presented in the main text, we believe that the same behavior is valid. In other words, the CNP positioned at $V_G^{ch} = -22V$ ($-29V$) for the curves present on Figure S8(a) (Figure S8(b)) is associated with the CNP for the graphene channel for 5nm (10nm) oxide thick. While $V_G^{cont} = -37V$ ($-45V$) is related with graphene underneath the electrodes.

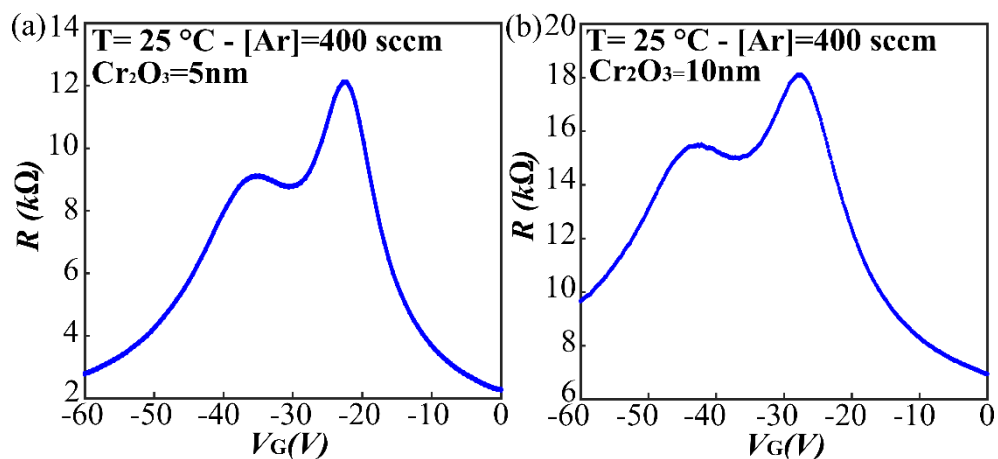


Figure S8. $R \times V_G$ in Ar atmosphere (400 sccm) at $T=25^\circ\text{C}$, for devices with 5 nm (a) and 10nm (b) of chromium oxide thick layer as stick layer for gold contacts.

Even though these devices exhibit double-CNP after fabrication in Argon atmosphere, when they are exposed to H₂ we observe a shift in both CNPs towards more negative gate value, indicating that both regions accept electrons (n-type doping) coming from the interaction with H₂ at the metal-graphene interface, as shown in Figure S9. One can note that initially the CNPs were positioned at $V_G^{ch} = -35V$ and $V_G^{cont} = -52V$ but after H₂ exposure the shifted to $V_G^{ch} = -43V$ and $V_G^{cont} < -60V$. These observations are also in agreement with our hypothesis that modifications at the metal-graphene interface can induce a large charge transfer to the graphene device.

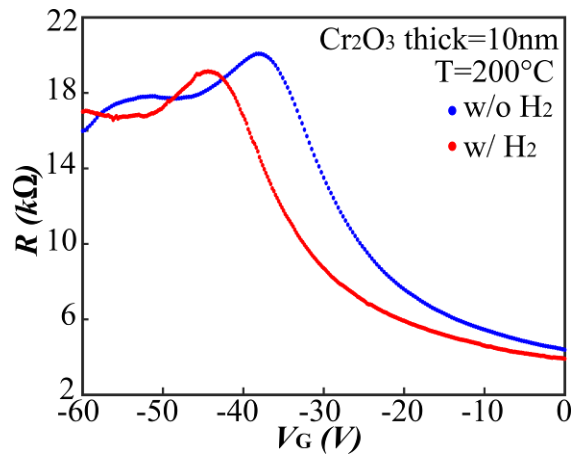


Figure S9. Two-probe RxV_G for the graphene device with 10nm Cr₂O₃ thick at $T=200^\circ C$. The blue curve presents the measurement without H₂, while the red curve shows the measurement with $[H_2]=20\%$ and after 1h of exposure.

5 – Changes in the contact resistance (R_C) under H₂ exposure

Figure S10 shows RxV_G curves without (Fig. S10(a)) and with (Fig. S10(b)) H₂ exposure. In our previous work, we observed that hydrogen molecules are able to tune the doping underneath the contact, modulating the pn junction due to changes on electrostatic interaction between graphene and contact [6]. Here, we demonstrate this phenomenon clearly, as discussed in the main text and also in Figure S10. The curves present an increasing on resistance for negative values of charge density (n) more accentuated than the positive values of n , due the formation of second CNP.

In the main text we analyzed changes in the contact resistance (R_C) under H₂ exposure (Figure 2(d)) for a fixed value of $n=-2.8 \times 10^{12} \text{cm}^{-2}$ (left side of the CNP in Figure

S10(b) marked by the dashed line). Now, we demonstrate that similar changes occur for values at $n = 1.45 \times 10^{12} \text{ cm}^{-2}$ (right side of the CNP in Figure S10(b) marked by the dashed line), where the fitted R_C values are $R_C^{\text{Ar}} = W \cdot (460 \pm 80) \Omega \mu\text{m}$ and $R_C^{\text{H}_2} = W \cdot (430 \pm 20) \Omega \mu\text{m}$ for without and with H_2 exposure, respectively. Therefore, one can notice that the GFETs exposed to H_2 depict lower contact resistance, indicating that R_C is affected by the molecules, $R_C^{\text{H}_2} / R_C^{\text{Ar}} \approx 93\%$. These results suggest that the H_2 molecules can significantly change the metal-graphene interface potential, as expected and discussed in the main text.

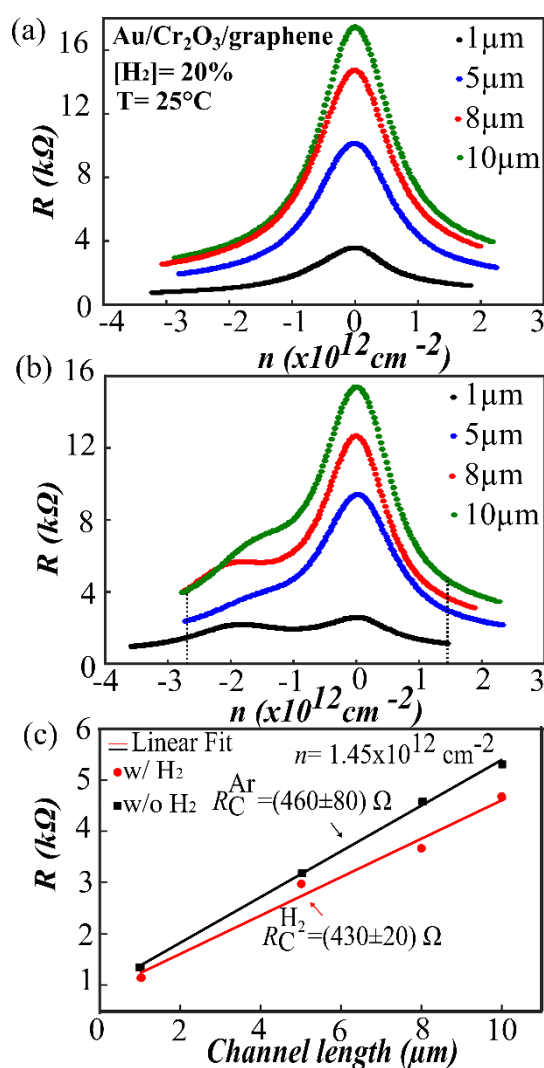


Figure S8. $R \times V_G$ for different channel length without normalization (a) without H_2 exposure and (b) with H_2 exposure. (c) $R \times$ Channel length w/ and w/o H_2 exposure.

This is the authors' version (pre peer-review) of the manuscript: C. L. Pereira et al 2D Materials
<https://doi.org/10.1088/2053-1583/ab0b23>

That has been published in its final form: <https://iopscience.iop.org/article/10.1088/2053-1583/ab0b23/meta>

REFERENCES

- [1] Moulder J F, Stickle W F, Sobol P E 1992 *Perkin-Elmer Corporation* vol 18
- [2] Chiu H Y, Perebeinos V, Lin Y M and Avouris P 2010 *Nano Letters* **10** 4634–9
- [3] Bartolomeo A Di, Giubileo F, Santandrea S, Romeo F, Citro R, Schroeder T and Lupina G 2011 *Nanotechnology* **22** 1-8
- [4] Nouchi R and Tanigaki K 2014 *Applied Physics Letters* **105** 1-12
- [5] Nouchi R and Tanigaki K 2010 *Applied Physics Letters* **96** 1–4
- [6] Cadore A R, Mania E, de Morais E A, Watanabe K, Taniguchi T, Lacerda R G and Campos L C 2016 *Applied Physics Letters* **109** 033109